**A&A manuscript no.**
(will be inserted by hand later)

**Your thesaurus codes are:**
**6(08.09.2 EV Lac; 08.12.1; 08.01.2; 08.03.5; 13.25.5)**

ASTRONOMY AND ASTROPHYSICS
September 9, 1999

# An extreme X-ray flare observed on EV Lac by ASCA in July 1998

**F. Favata[1], F. Reale[2], G. Micela[3], S. Sciortino[3], A. Maggio[3], and H. Matsumoto[4]**

[1] Astrophysics Division – Space Science Department of ESA, ESTEC, Postbus 299, NL-2200 AG Noordwijk, The Netherlands
[2] Dip. Scienze FF. & AA., Sez. Astronomia, Univ. Palermo, Piazza del Parlamento 1, I-90134 Palermo, Italy
[3] Osservatorio Astronomico di Palermo, Piazza del Parlamento 1, I-90134 Palermo, Italy
[4] Center for Space Research – Massachusetts Institute of Technology, 77 Massachusetts Avenue, 02139 Cambridge (MA), USA

Received date ; accepted date

**Abstract.** We present a long (150 ks elapsed time) X-ray observation of the dM3.5e star EV Lac, performed with the ASCA observatory in July 1998, during which an exceptionally intense flaring event (lasting approximately 12 ks) was observed; at the flare's peak, the X-ray count rate in the ASCA GIS detectors was $\simeq 300$ times the quiescent value. The physical parameters of the flaring region have been derived by analyzing the decay, using both a "classic" quasi-static approach and an approach based on hydrodynamic simulations of decaying flaring loops. Notwithstanding the large peak X-ray luminosity, this second method shows that the flare's decay is compatible with its being produced in a relatively compact region of semi-length $L \simeq 1.3 \times 10^{10}$ cm ($\simeq 0.5\ R_*$), large but not exceptional even by solar standards. The flare decays is fast (with a measured $e$-folding time for the light curve of $\leq 2$ ks), but nevertheless the hydrodynamic-based analysis shows strong evidence for sustained heating, with the shape of the light curve dominated by the time evolution of the heating rather than by the natural cooling of the flaring plasma. As a consequence, the quasi-static method yields a much larger estimate of the loop's length ($L \simeq 2\ R_*$). The event shows (similarly to some other well-studied large stellar flares) a light curve characterized by two separate decay time constants (with the initial decay being faster) and a significant enhancement in the plasma metal abundance at the peak of the flare. The energetics of the event are exceptional, with the peak X-ray luminosity of the event reaching up to $\simeq 25\%$ of the bolometric luminosity of the star, making this the largest X-ray flare (in relative terms) observed to date on a main-sequence star.

**Key words:** Stars: individual: EV Lac – Stars: late-type – Stars: activity – Stars: coronae; X-rays: stars

## 1. Introduction

One of the basic standing problems of stellar coronal astronomy is the determination of the spatial structuring of the coronal plasma. While for the study of stellar interior structure the first-order approximation of spherical symmetry is a good starting point, stellar coronae are, as shown by the large body of extant imaging observations of the solar corona, far from spherically symmetric. The solar corona shows a high degree of spatial structuring: most of the X-ray luminous plasma is confined in coronal loops preferentially located at mid-latitudes, with an average location which tracks the migration of sunspots through the solar cycle. The lack of spatial information constitutes a strong limitation for the study of stellar coronae: low-resolution X-ray spectra of coronal plasmas are insensitive to the plasma's density, so that non-dispersive, CCD- or proportional counter-based spectral observations do not allow to distinguish between a large diffuse corona and a compact, structured, high-pressure one. It is thus not possible, if the solar analogy is postulated, to determine how the solar corona scales toward higher levels of activity, i.e. if largely through a spatial filling of the available volume with coronal loops (yielding a relatively symmetric corona) or if through the filling of a relatively small number of coronal structures with significantly higher density plasma.

Thus far the main tools to study the spatial distributions of the coronal plasma have been eclipse experiments and the study of flares. While the observation of rotational modulation should also in principle allow to derive the spatial distribution of the emitting plasma, as discussed by Schmitt (1998) convincing examples of rotationally modulated X-ray emission are rare. Under a given set of assumptions, the study of the decay phase of a flare can yield information about the size of the flaring structure; different methods for this type of analysis have been developed and applied in the past to several observations of stellar flares. The widely applied quasi-static approach (see below) almost invariably results, when applied to intense stellar flares, in long, tenuous coronal loops extending out to several stellar radii. The stronger flares yield in general larger sizes. Detailed hydrodynamic modeling of flaring loops has provided useful insight on stellar X-ray flares (Reale et al. 1988); more recently diagnostic tools have been developed for the derivation of the size of stellar flaring loops and of the heating evolution (Reale et al. 1993; Reale et al. 1997; Reale & Micela 1998). In the solar case, in addition to the "compact" flares, in which the plasma appears to be confined to a single loop whose geometry does not significantly evolve during the event (an assumption

*Send offprint requests to*: F. Favata (ffavata@astro.estec.esa.nl)

shared by the quasi-static method and by the hydrodynamic modeling quoted above), a second class of flares is usually recognized, i.e. the "two-ribbon" events, in which an entire arcade of loops first opens and then closes back; the footpoints of the growing system of loops are anchored in H$\alpha$-bright "ribbons". These flares are generally characterized by a slower rise and decay, and a larger energy release. Compact flares have often been considered to be due to "impulsive" heating events, while the longer decay times of two-ribbon events have been considered as a sign of sustained heating. However, also in the case of compact flares sustained heating has been shown to be frequently present (Reale et al. 1997), so that the distinction may indeed be less clear than often thought.

Fitting of X-ray spectra with physical models of static loops (Maggio & Peres 1997; Sciortino et al. 1999) can also yield the surface filling factor of the plasma as one of the fit parameters. However, for loops smaller than the pressure scale height this method only gives an upper limit to the filling factor, which needs to be further constrained, for example, with estimates of the plasma density based on EUV line ratios (Maggio & Peres 1997). With few exceptions (notably the observation of $\alpha$ CrB, Schmitt & Kurster 1993, in which the observed total eclipse constrains the corona on the G5V star to have a scale height much less than a solar radius), eclipse studies of the quiescent emission of eclipsing binaries have thus far failed to yield strong constraints on spatial structuring of the plasma (Schmitt 1998). In part this is due to the inversion of the weak observed modulation being mathematically an intrinsically ill-posed problem, where few compact structures can mimic the emission from a more diffuse medium (see discussion in Schmitt 1998). Recently, the observation of the total eclipse of a large flare on Algol (Schmitt & Favata 1999) has for the first time yielded a strong geometrical constraint on the size of a flaring structure. The geometrical loop size is significantly smaller than the size derived from the analysis of the flare's decay (Favata & Schmitt 1999) using the quasi-static method, showing how such approach can over-estimate the actual loop size. The characteristics of the Algol flare are such that the hydrodynamic decay, sustained heating framework which we also use here yields a large range of allowed loop semi-lengths, with the lower end of the range marginally compatible with the geometrically derived size.

The presence of intense X-ray flares on flare stars[1] was well established with *Einstein* observations – with some by now classic observations such as the one relative to a flare on Proxima Cen (Haisch 1983). However, *Einstein* observations were usually relatively short (few ks) thus imposing a bias on the type of events which could be detected (Ambruster et al. 1987). In particular, the short total integration times reduced the chance of detecting rare event types. The EXOSAT observatory featured long, uninterrupted observations, and thus allowed to collect a more unbiased view of flares on low-mass stars, resulting in a database (Pallavicini et al. 1990) of about 300 hr of flare stars observations, from which it is apparent that flares come in a large variety of sizes for both their time scales and their energetics. Pallavicini et al. (1990) did not attempt to derive the spatial scales of the observed flares, although they tentatively divided them into two classes reminiscent of the solar compact and two-ribbon flares. The next generation of of flare observations came with the ROSAT All-Sky Survey (RASS), which, thanks to its sky scanning strategy, allowed to search for rare, long-lasting events. Some flares of previously undetected magnitude and duration are indeed present in it (Schmitt 1994); in particular, EV Lac showed a long X-ray flare lasting approximately a day, superimposed on a much shorter but more intense event.

We have observed EV Lac for two days with the ASCA observatory, detecting the most intense X-ray flare thus far observed on a main-sequence star, with a 300-fold peak increase of the X-ray count rate. This paper presents a detailed analysis of the flaring event, and it is organized as follows: the ASCA observations and their reduction, together with the determination of the spectral parameters for the flare are discussed in Sect. 2, the parameters of the flaring region are determined (using both the quasi-static formalism of van den Oord & Mewe 1989 and the hydrodynamic decay, sustained heating framework of Reale et al. 1997) in Sect. 3, with a discussion (Sect. 4) closing the paper.

## 2. Observations and data reduction

EV Lac was observed by ASCA continuously for $\simeq$ 150 ks from 13 July 1998 06:10 UT to 15 July 1998 01:40 UT, as an AO-6 guest investigator target (P.I. F. Favata). The data were analyzed using the FTOOLS 4.1 software, extracting both the spectra and the light curves with the XSELECT package and performing the spectral analysis with the XSPEC 10.0 package. The MEKAL plasma emission model (Mewe et al. 1995) was adopted for the spectral analysis. The peak count-rate of the flare ($\simeq$ 100 cts s$^{-1}$ in the SIS) exceeds both the telemetry limit ($\simeq$ 40 cts s$^{-1}$) and the 1% pile-up limit throughout the whole point-spread function ($\simeq$ 60 cts s$^{-1}$), thus preventing a reliable spectroscopic analysis. We therefore only uses the GIS data in the following. Source photons have been extracted, for both GIS-2 and GIS-3 detectors, from a circular region 18.5 arcmin in diameter (74 pixels, somewhat larger than the suggested extraction radius for GIS data; given the strength of the source this ensures that as many as possible source photons are collected) centered on the source position, while background photons have been extracted from a circular region identical in size to the source region but symmetrically placed with respect to the optical axis of the X-ray telescope. For point sources such strategy allows for the background to be extracted from the same observation (and thus with the same screening criteria) while ensuring that the effect of telescope vignetting on cosmic background photons is properly accounted for. Given the high intensity of the source emission during the flare, the background is however effectively negligible. The

[1] We use the term to mean "M-type dwarfs, either single or members of a multiple system, which show frequent sudden enhancements of their X-ray, UV and optical luminosity".

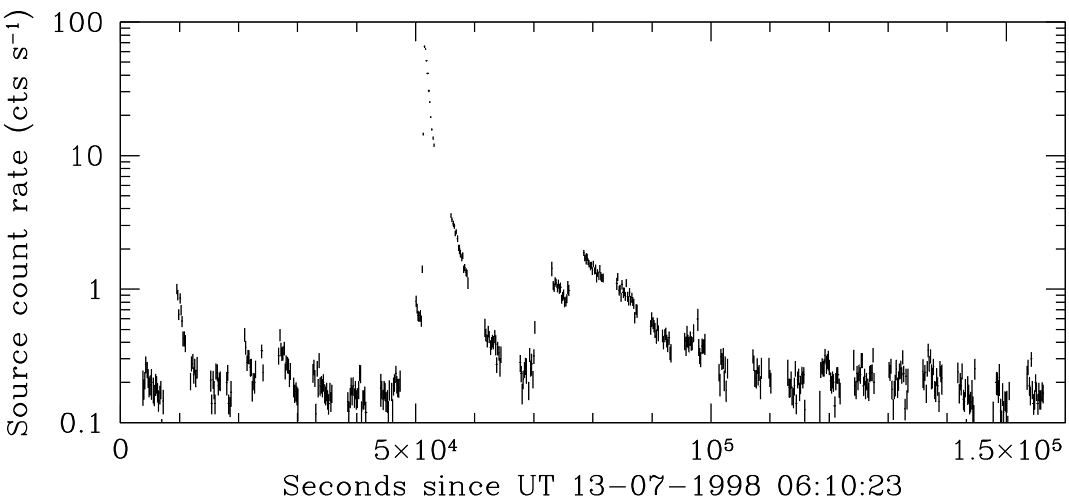


**Fig. 1.** The background-subtracted (background count rate $\simeq$ 0.05 cts s$^{-1}$) GIS-3 light curve of EV Lac for the entire ASCA observation, binned in 180 s intervals.

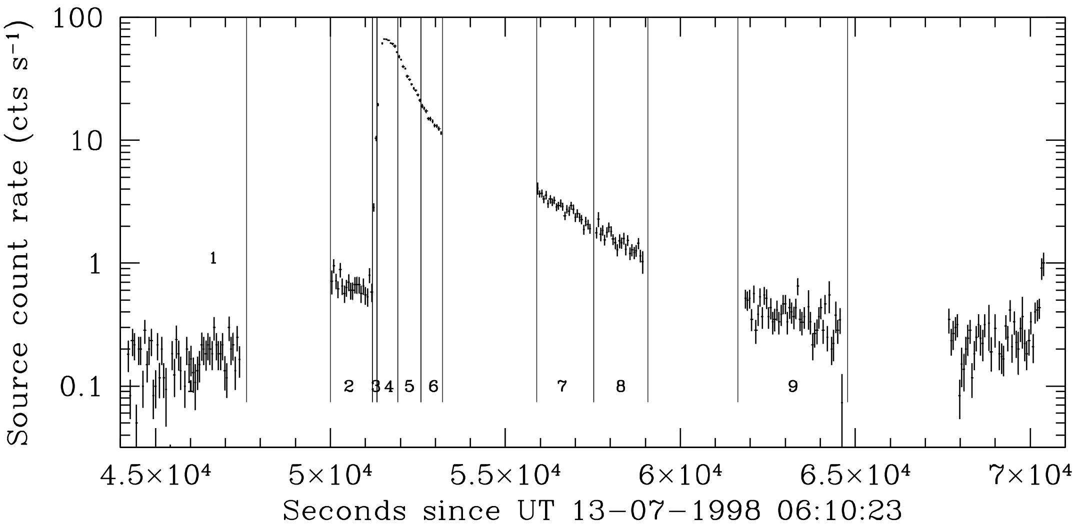


**Fig. 2.** The background-subtracted (background count rate $\simeq$ 0.05 cts s$^{-1}$) GIS-3 light curve of the large EV Lac flare discussed in the present paper, binned in 60 s intervals. The extent of the time intervals in which the flare has been divided for the determination of the flare's spectral parameters is shown. No dead time correction has been applied to the count rates.

GIS-3 background-subtracted light curve for EV Lac for the complete duration of the ASCA observation is shown in Fig. 1.

The light curve shows evidence for variability on many time scales, and at least three individual flares can be identified: the exceptional event at $\simeq$ 51 ks from the beginning of the observation, and two minor (however still rather sizable) flares at $\simeq$ 10 and $\simeq$ 75 ks. The light curves of both minor events show a clear exponential decay, but their peak is not covered by the observations. To derive the temporal evolution of the temperature and emission measure of the large flare we have subdivided it in 9 time intervals, shown together with the GIS-3 light curve of the event in Fig. 2. Individual GIS-2 and GIS-3 spectra have been extracted for each of these intervals and merged using the procedure described in the ASCA ABC Guide (1997). The exposure time of each individual spectrum has been corrected for the dead-time of the GIS (which, at these high count rates is rather significant, with values up to 1.2 – note that the both light curves from Figs. 1 and 2 are *not* corrected for detector dead-time). The quiescent spectrum has been taken from the interval immediately preceding the flare (interval 1 in Fig. 2, covering $\simeq 5$ ks). A two-temperature model has been fit to the spectrum extracted from interval 1, with the resulting spectral parameters shown in Table 1.

**Table 1.** The spectral parameters derived for the quiescent emission of EV Lac from the analysis of the GIS-2 and GIS-3 spectra accumulated during the time interval 1, using a two-temperature MEKAL spectral model. The fit has 72 degrees of freedom, and the corresponding probability level is 99.8%. The quiescent X-ray luminosity corresponding to the above spectral parameters is $L_X = 3 \times 10^{28}$ erg s$^{-1}$.

| $T_1$ | $T_2$ | $EM_1$ | $EM_2$ | $Z$ | $\chi^2$ |
|---|---|---|---|---|---|
| keV | | $10^{51}$ cm$^{-3}$ | | $Z_\odot$ | |
| $0.78 \pm 0.15$ | $1.92 \pm 1.2$ | 2.35 | 0.76 | 0.29 | 0.97 |

The sequence of GIS flare spectra is shown in Fig. 3. The left panel shows the spectra collected during the rising phase of the flare, up to the peak in the light-curve (interval 4), while the decay-phase spectra are plotted in the right panel. Individual flare spectra from time intervals 2 to 9 have been fit with a single-temperature MEKAL model; given the lack of soft response in the GIS no absorbing column density was included. The quiescent emission was modeled by adding a frozen-parameter two-temperature MEKAL model to the fit (with the parameters as in Table 1); the results of the spectral fits are shown in Table 2. During intervals 5 and 6 the single-temperature fit does not yield a satisfactory reduced $\chi^2$ (see Table 2), due to the large residuals present in the region around 1 keV, with the observed spectra showing some additional emissivity with respect to the models. Similar effects are also seen in the in the ASCA SIS Capella spectrum (Brickhouse 1998) and in the flaring spectra of Algol as seen by SAX (Favata & Schmitt 1999), suggesting that current plasma emission codes (as the MEKAL one used here) can under-predict the observed spectrum around 1 keV, likely due to a large number of high quantum-number ($n > 5$) Fe L lines from Fe XVII, Fe XVIII and Fe XIX (Brickhouse 1998), and thus the formally unacceptable $\chi^2$ resulting from the fit does not necessarily imply that the one-temperature model is not correctly describing the observed spectrum. Indeed, we have verified that adding further temperature components does not significantly improve the fit for intervals 5 and 6. The time evolution of the flare's spectral parameters (temperature, emission measure, plasma metal abundance) is shown in Fig. 4, together with the flare's GIS-3 light-curve binned in the same time intervals.

## 3. Flare analysis

We have analyzed the present flare using two different frameworks (quasi-static cooling and hydrodynamic decay, sustained heating), which both make the assumption that the flaring plasma is confined in a closed loop structure, whose geometry is not significantly evolving during the event. Although direct support to this assumption is of course missing, the relatively short duration of the event allows an analogy with solar compact flares. In any case the second method provides reliable scale sizes of the flaring structure even in the presence of some readjustment of the magnetic field, the crucial assumption been plasma confinement.

### *3.1. The quasi-static cooling framework*

Many stellar X-ray flares observed to date have been studied using the quasi-static formalism first discussed in detail by van den Oord & Mewe (1989). It is thus of interest to analyze the present event with the quasi-static approach, to allow a homogeneous comparison with literature data, even if, as discussed by Favata & Schmitt (1999), this method can significantly over-estimate the size of the flaring loops (see also Reale et al. 1997).

According to van den Oord & Mewe (1989), for the decay to be quasi-static (i.e. to happen through a sequence of states each of which can be described by the scaling laws applicable to stationary coronal loops) the ratio between the characteristics times for radiative and conductive cooling must be constant during the flare decay (although its absolute value needs not be known). This ratio is parameterized by the quantity

$$\mu = \frac{\tau_r}{\tau_c} = C \times \frac{T^{13/4}}{EM}, \qquad (1)$$

The normalization $C$ depends on the details of the loop's geometry, and is not relevant here. The evolution of $\mu$ is plotted in Fig. 5; within the error bars $\mu$ is constant during the whole decay, so that the conditions for the applicability of the quasi-static decay framework are in this case met.

The scaling laws discussed by Stern et al. (1992) –linking the loop semi-length $L$ and the plasma density $n$ with the peak flare temperature $T$ and the effective decay time $\tau$ – yield results very similar to the ones obtained through a full fit to the equations of van den Oord & Mewe (1989), so that we will limit ourselves to their application. Specifically, $L \propto \tau T^{7/8}$ and $n \propto \tau^{-1} T^{6/8}$, valid for temperature regimes in which the plasma emissivity scales as $\Psi_0 T^{-\gamma}$ with $\gamma \simeq -0.25$. In practice this is valid for $T \gtrsim 20$ MK, i.e. for most of the decay of the flare discussed here. Scaling the values determined for the EV Lac flare from the parameters derived by van den Oord & Mewe (1989) for the EXOSAT flare observed on Algol, the derived loop semi-length is $L \simeq 5 \times 10^{10}$ cm ($\simeq 2\ R_*$), and the plasma density $n \simeq 6 \times 10^{11}$ cm$^{-3}$.

### *3.2. The hydrodynamic decay, sustained heating framework*

A different approach to the study of a flare's decay phase, with the same aim of determining the physical parameters of the flaring region, has been developed by Reale et al. (1997). It has been recognized from the modeling of solar X-ray flares that the slope of the locus of the flare decay in the $\log n$–$\log T$ plane is a powerful diagnostic of the presence of additional heating

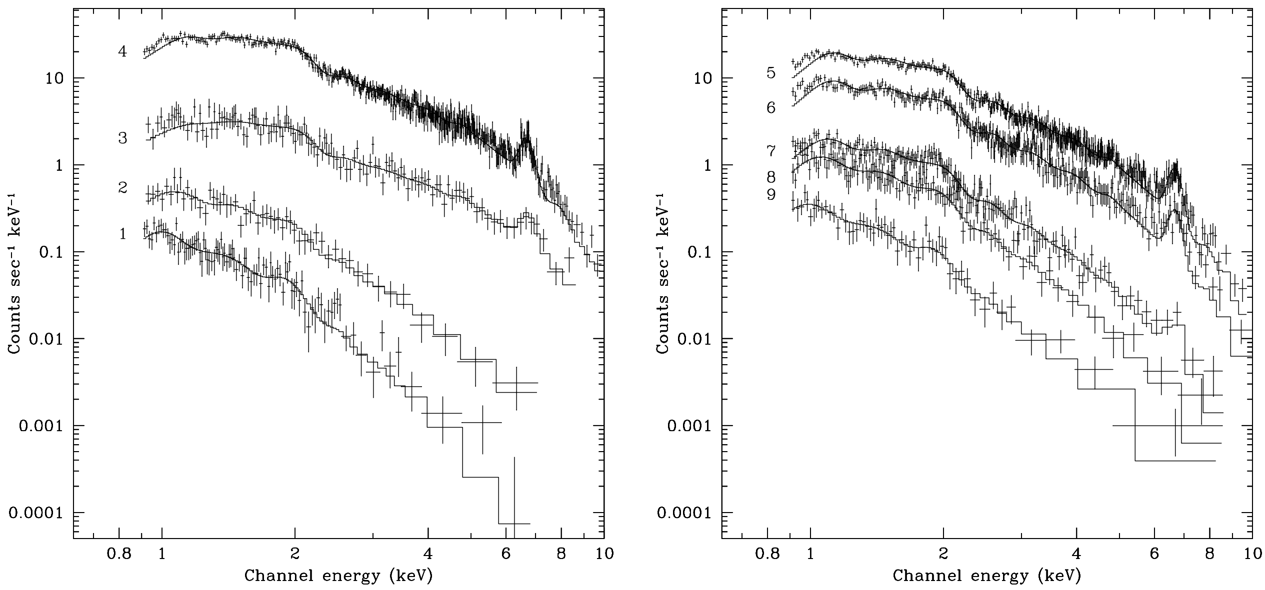


**Fig. 3.** The time sequence of merged (GIS-2 + GIS-3) spectra for the EV Lac flare. The left panel shows the sequence of spectra during the rise phase of the flare, up to its peak, while the right panel shows the sequence of decay spectra. The numeric label at the left of each spectrum indicates the time interval during which the spectrum was collected, as numbered in Fig. 2. Each spectrum is overplotted with the corresponding best-fit model from which the spectral parameters have been derived. The spectra have been rebinned to a minimum signal-to-noise ratio per bin of 2.

**Table 2.** The spectral parameters $T$, $Z$ and $EM$ derived for the individual phases of the EV Lac flare from the analysis of the GIS spectra accumulated during the time intervals 2 to 9. The spectra have been analyzed with a single-temperature MEKAL model (plus a frozen-parameter two-temperature model to account for the quiescent emission). The bounds of the confidence intervals at the 90% levels ($\Delta\chi^2 = 3.5$) are also reported for each parameter. The time interval $i$ for which each set of parameters applies is shown in Fig. 2.

| $i$ | $T$ | $T_{+90\%}$ | $T_{-90\%}$ | $Z$ | $Z_{+90\%}$ | $Z_{-90\%}$ | $EM$ | $EM_{+90\%}$ | $EM_{-90\%}$ | $\chi^2$ | DoF | Prob. |
|---|---|---|---|---|---|---|---|---|---|---|---|---|
| | | keV | | | $Z_\odot$ | | | $10^{53}$ cm$^{-3}$ | | | | |
| 2 | 1.65 | 1.37 | 1.96 | 0.36 | 0.08 | 1.20 | 0.075 | 0.044 | 0.11 | 30.1 | 57 | 0.995 |
| 3 | 6.33 | 5.37 | 7.42 | 0.64 | 0.33 | 0.97 | 0.79 | 0.75 | 0.85 | 88.1 | 128 | 0.995 |
| 4 | 3.98 | 3.88 | 4.08 | 0.64 | 0.56 | 0.72 | 7.35 | 7.19 | 7.54 | 481.0 | 468 | 0.294 |
| 5 | 2.92 | 2.86 | 2.98 | 0.86 | 0.76 | 0.95 | 3.83 | 3.71 | 3.96 | 561.2 | 417 | $< 0.01$ |
| 6 | 2.54 | 2.46 | 2.61 | 0.77 | 0.63 | 0.91 | 1.73 | 1.63 | 1.85 | 391.1 | 297 | $< 0.01$ |
| 7 | 1.72 | 1.62 | 1.82 | 0.35 | 0.23 | 0.50 | 0.41 | 0.35 | 0.47 | 190.1 | 183 | 0.27 |
| 8 | 1.29 | 1.17 | 1.42 | 0.21 | 0.11 | 0.39 | 0.25 | 0.20 | 0.31 | 99.0 | 117 | 0.84 |
| 9 | 0.91 | 0.70 | 1.17 | 0.15 | 0.05 | 0.50 | 0.047 | 0.022 | 0.088 | 50.8 | 67 | 0.88 |

during the decay itself (Sylwester et al. 1993); by making use of extensive hydrodynamic modeling of decaying flaring loops, with different heating time scales, Reale et al. (1997) have derived an empirical relationship between the light curve decay time (in units of $\tau_{\rm th}$, the loop thermodynamic decay time, Serio et al. 1991) and the slope $\zeta$ in the $\log n$–$\log T$ diagram. This allows to derive the length of the flaring loop length as a function of observable quantities, i.e. the decay time of the light curve, the flare maximum temperature and the slope of the decay in the $\log n$–$\log T$ diagram (the square root of the emission measure of the flaring plasma is actually used as a proxy to the density). Since the characteristics of the observed decay depend on the specific instrument response, the parameters of the actual formulas used have to be calibrated for the telescope used to observe the flare.

The method reported in Reale et al. (1997) was tested on a sample of solar flares observed with Yohkoh-SXT, for which both images (from which the length of the flaring loop was measured) and spectral parameters (from the temperature and emission measure diagnostic derived from Yohkoh filter ratios) were available, and has been shown to provide reliable results for most of the studied events. A first application of the method to stellar flares observed with ROSAT PSPC is described by Reale & Micela (1998).

For the present study the method has been recalibrated for stellar flares observed with ASCA GIS. The thermodynamic decay time $\tau_{\rm th}$ of a closed coronal loop with semi-length $L$,

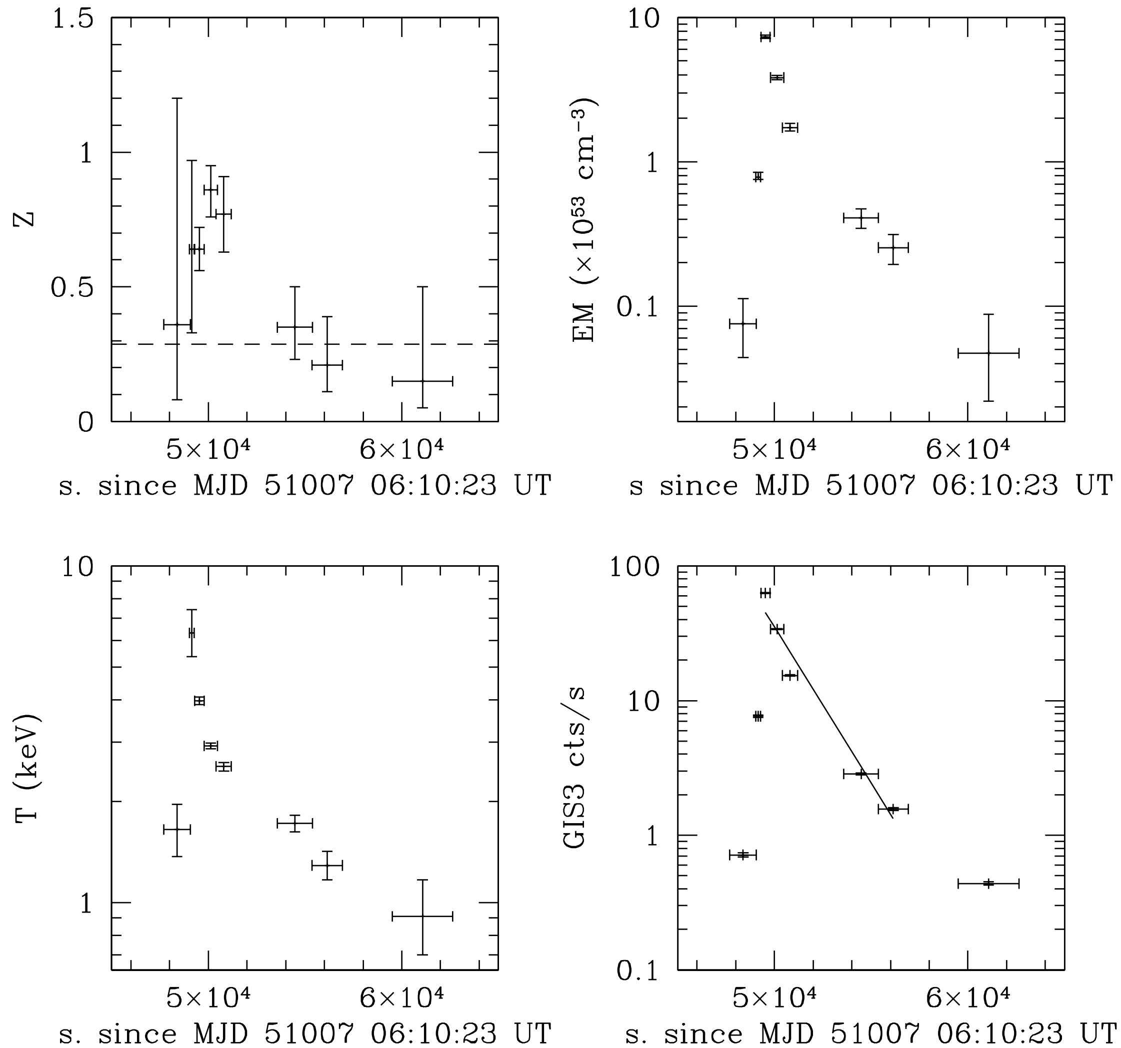


**Fig. 4.** The temporal evolution of the spectral parameters of the flare, i.e. the plasma metal abundance (top left), emission measure (top right) and temperature (bottom left). Also shown (bottom right), the light-curve of the flare as seen by the GIS-3 detector, integrated in the same temporal intervals as the ones used to extract the flare's spectra. The best-fit exponential decay to the light curve is also plotted. The dashed horizontal line in the abundance plot represents the value of the metal abundance determined for the quiescent, pre-flare spectrum.

and maximum temperature $T_{\max}$ is given by Serio et al. (1991) as

$$\tau_{\rm th} = \frac{\alpha L}{\sqrt{T_{\max}}} \quad (2)$$

where $\alpha = 3.7 \times 10^{-4}$ cm$^{-1}$ s$^{-1}$ K$^{1/2}$. By means of a grid of hydrostatic loop models (see Reale & Micela 1998) we have determined an empirical relationship linking the loop maximum temperature $T_{\max}$, typically found at the loop apex (e.g. Rosner et al. 1978) to the maximum temperature $T_{\rm obs}$ determined from the GIS spectrum:

$$T_{\max} = 0.085 \times T_{\rm obs}^{1.176} \quad (3)$$

Following the same procedure as in Reale et al. (1997) and Reale & Micela (1998) (using extensive hydrodynamic modeling of decaying flaring loops) we have determined the ratio between $\tau_{\rm LC}$ (the observed $e$-folding time of the flare's light curve determined by fitting the light curve from the peak of the flare down to the 10% of peak level) and $\tau_{\rm th}$ as a function of the slope $\zeta$ in the $\log \sqrt{EM}$–$\log T$ diagram to be, for the ASCA GIS

$$\frac{\tau_{\rm LC}}{\tau_{\rm th}} = F(\zeta) = c_a e^{-\zeta/\zeta_a} + q_a \quad (4)$$

where $c_a = 10.9$, $\zeta_a = 0.56$ and $q_a = 0.6$. The formula for the loop semi-length $L$ is therefore:

$$L = \frac{\tau_{\rm LC}\sqrt{T_{\max}}}{\alpha F(\zeta)} \qquad 0.38 < \zeta \leq 1.7 \quad (5)$$

where the second part of the relationship gives the range of $\zeta$ values allowed according to the modeling. The uncertainty on

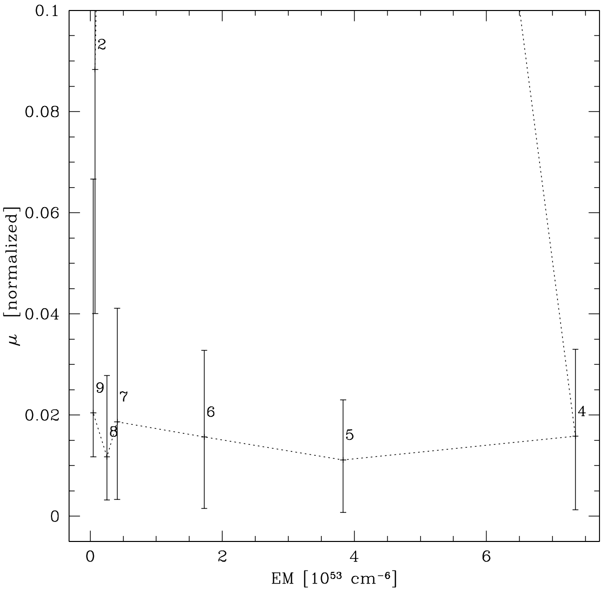


**Fig. 5.** The temporal evolution of the $\mu$ parameter (the ratio between the radiative and conductive cooling time for the loop) during the flare. The dotted line joins the points corresponding to the different time intervals reported in Fig. 2.

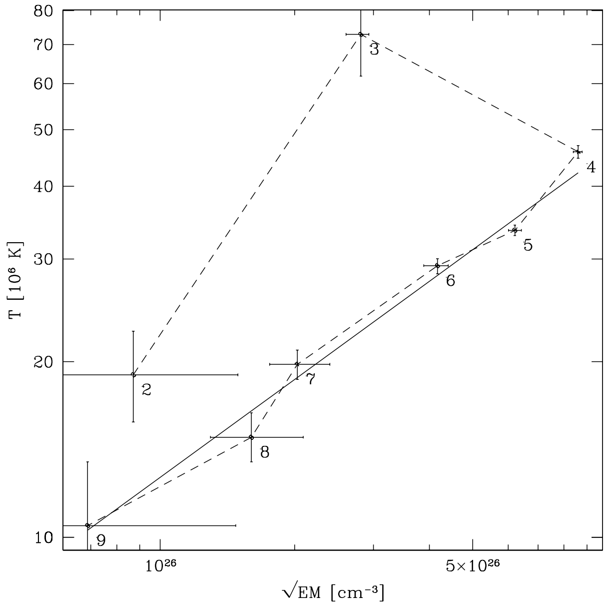


**Fig. 6.** The evolution of the flare's decay in the $\log\sqrt{EM}$–$\log T$ plane. The points plotted represent the flare's evolution from time interval 2 to time interval 9 inclusive. The dotted line joins the points corresponding to successive intervals. The decay phase begins with the third interval, and it closely follows a straight line. The continuous line is a least-square fit to the decay phase, with a best-fit slope $\zeta = 0.56 \pm 0.04$, while the numeric labels indicate the time interval to which each point refers.

$L$ is the sum of the propagation of the errors on the observed parameters $\tau_{\rm LC}$ and $\zeta$ with the standard deviation of the difference between the true and the derived loop lengths. The latter amounts to $\simeq 15\%$. Equation 5 has been tuned on exponentially decaying light curves; however it has been shown to provide reliable results also on solar flares with more complex decay trends, e.g. a double exponential decay (as for the flare studied here), provided that the whole decay is fitted with a single exponential (F. Reale, private communication).

The evolution of the EV Lac flare in the $\log\sqrt{EM}$–$\log T$ plane is shown in Fig. 6, together with a least-square fit to the decay phase. The resulting best-fit slope for the decaying phase computed for time intervals from 4 to 9 inclusive is $\zeta = 0.56 \pm 0.04$. Application of Eq. 4 yields a ratio between the observed cooling time scale $\tau_{\rm LC}$ and the thermodynamic cooling time scale for the flaring loop $\tau_{\rm th}$ of $F(\zeta) = 4.6$. Such a large value implies that the observed decay is driven by the time-evolution of the heating process and not by the free cooling of the loop. Also, the actual loop length will be significantly smaller than it would be estimated assuming that the spectral parameters reflect free cooling of the decaying loop. The actual value of $\tau_{\rm LC}$ has been determined by fitting the GIS light curve, binned in the same time intervals used for extracting the individual flare spectra (as plotted in Fig. 2), considering the intervals from 4 to 9 inclusive. In this case $\tau_{\rm LC} = 1.80 \pm 0.15$ ks, and therefore $\tau_{\rm th} \simeq 400$ s. The intrinsic flare peak temperature is, applying Eq. 3 to the observed maximum temperature, $T_{\max} \simeq 150$ MK. From Eq. 5 the loop semi-length is $L = (1.3 \pm 0.3) \times 10^{10}$ cm, i.e. $L \simeq 0.5\, R_*$. This loop length is much smaller than the pressure scale height[2] of the flaring plasma on EV Lac and also significantly smaller (by a factor of 4) than the one derived through the quasi-static formalism.

A simple consistency check can be obtained by comparing the pressure obtained by assuming that the flaring loop is not, at maximum, far from a steady-state condition (thus applying the scaling laws of Rosner et al. 1978) with the pressure implied by the derived values of $L$ and $T$ for a plausible geometry. In practice the geometry is parameterized by the ratio $\beta$ between the radius of the loop and its lenght. The pressure is then

$$n = \sqrt{\frac{EM}{2\pi L^3 \beta^2}} \tag{6}$$

If we assume $\beta \simeq 0.1$–$0.3$ (a typical range for solar coronal loops) the loop volume is $\simeq 1.4$–$13 \times 10^{29}$ cm$^3$, and the resulting plasma density at the peak of the flare is $n \simeq 2$–$0.2 \times 10^{12}$ cm$^{-3}$. The corresponding pressure is $p_{\max} \simeq 8$–$0.9 \times 10^4$ dyne cm$^{-2}$. Using the scaling laws of Rosner et al. (1978) applicable to steady-state loops,

$$T_{\max} = 1.4 \times 10^3 (p_0 L)^{1/3} \tag{7}$$

[2] defined as $H = 2kT/\mu g$, where T is the plasma temperature in the loop, $\mu$ is the molecular weight and $g$ is the surface gravity of the star. In this case $H \simeq 8 \times 10^{11}$ cm

where $p_0$ is the pressure at the base of the loop, one obtains $p_0 \simeq 10^5$ dyne cm$^{-2}$, slightly larger than $p_{\max}$ for $(\beta = 0.1)$. This implies that the plasma evaporated from the chromosphere has not $(\beta = 0.3)$ or nearly $(\beta = 0.1)$ filled the flaring loop up to the hydrostatic equilibrium conditions at flare maximum.

### 3.3. Energetics

We have computed, for each of the 8 time intervals in which the flare has been subdivided, the X-ray luminosity in the 0.1–10. keV band. For this purpose the spectrum has been extrapolated outside of the formal spectral range covered by the GIS detectors; this is at most likely to underestimate the true luminosity in the extended band, as it may miss any softer component present in the spectrum and invisible to the GIS. The time-evolution of the flare X-ray luminosity is shown in Fig. 7, in which the data are plotted both in absolute units and in units of the star's bolometric luminosity.

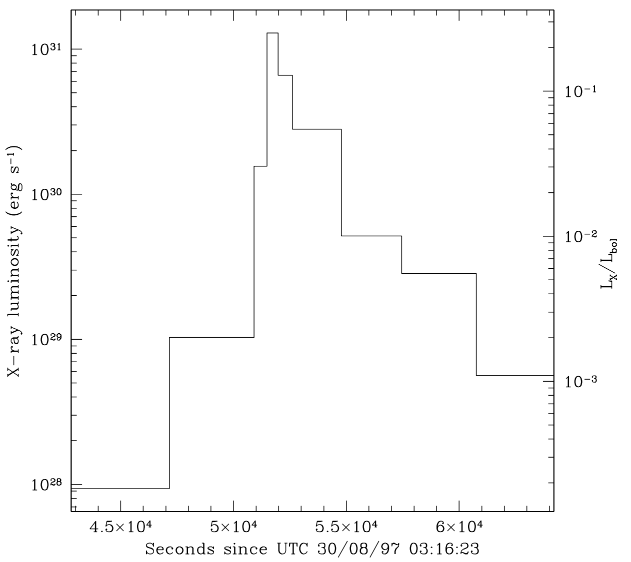


**Fig. 7.** The temporal evolution of the flare's X-ray luminosity calculated in the 0.1 to 10. keV band starting from the quiescent state. The left axis gives the luminosity in erg s$^{-1}$, while the right axis shows the same value in units of the star's bolometric luminosity ($5.25 \times 10^{31}$ erg s$^{-1}$).

During interval 4 (at the peak of the light curve) the X-ray luminosity of the flare is about one quarter of the photospheric (bolometric) luminosity of the star. Soft X-ray radiation is only one of the energy loss terms for the flaring plasma, with kinetic energy, conduction to the chromosphere and white light, UV and XUV flaring emission also significantly contributing to the energy budget. In the solar case, detailed analyses of flares of different types (Wu et al. 1986) show that at the peak of the event soft X-ray radiation only accounts for 10–20% of the total energy budget; similarly, Houdebine et al. (1993) analyzed a large optical flare on the dMe star AD Leo, concluding that the kinetic energy of plasma's motions during the event is likely to be at least as large as the radiated energy during the flare.

A detailed assessment of the energy balance of the present flare is not possible, given the lack of multi-wavelength coverage and of velocity information which could help assessing the plasma kinetic energy. The total energy radiated in the X-rays is $E \simeq 1.5 \times 10^{34}$ erg (obtained with simple trapezoidal integration of the instantaneous X-ray luminosity), over $\simeq$ 10 ks, equivalent to $\simeq$ 300 s of the star's bolometric energy output. From the scaling laws of Rosner et al. (1978) we can estimate the heating rate per unit volume at the peak of the flare, assumed uniform along the loop, as

$$\frac{dH}{dV dt} \simeq 10^5\, p^{7/6}\, L^{-5/6} \simeq 240 \text{ erg cm}^{-3}\text{ s}^{-1} \quad (8)$$

The total heating rate at the flare maximum is therefore

$$\frac{dH}{dt} \simeq \frac{dH}{dV dt} \times V \simeq 3.3 \times 10^{31} \text{ erg s}^{-1} \quad (9)$$

a factor of $\simeq$ 3 higher than the flare maximum X-ray luminosity (see Fig. 7), compatible with X-ray radiation being only one of the energy loss terms during the flare. If we assume that the heating is constant for the initial rising phase, which lasts for $t_{\rm r} \simeq$ 300 s, and then decays exponentially, with an $e$-folding time $\tau_{\rm H} \simeq 4.6\tau_{\rm th} \simeq$ 1800 s (i.e. similar to $\tau_{\rm LC}$), the total energy released during the flare is

$$H_{\rm tot} \simeq \frac{dH}{dt} \times (t_r + \tau) \simeq 7 \times 10^{34} \text{ erg} \quad (10)$$

approximately five times the energy radiated in X-rays. Energy losses by thermal conduction are indeed expected to be large at such high temperatures.

### 3.4. Metal abundance

The metal abundance of the flaring plasma shows a significant evolution, rising, at the peak of the flare, to a value $\simeq$ 2 times higher than the abundance measured for the quiescent emission, and decaying back to the quiescent value during the terminal phase of the flare. Evolution of the metal abundance has been observed also in other flares – most clearly in the Algol flare observed with SAX, Favata & Schmitt (1999) – and the behavior observed here appears to follow the same general pattern of abundance enhancement going in parallel with the flare's light curve. The simplest explanation suggested for this has been to assume that a fractionation mechanism is at work in the quiescent corona, and that the evaporation of pristine photospheric material during the flare temporarily sets the coronal chemical equilibrium off balance. Unfortunately, few reliable abundance determinations are available for M dwarfs; in particular, no state-of-the-art photospheric abundance analysis of EV Lac is known to us, and thus it is not possible to assess whether the quiescent coronal abundance is indeed depleted with respect to the photospheric value.

## 4. Discussion

The most remarkable characteristic of the EV Lac flare discussed in the present paper is certainly its very large X-ray luminosity: at flare peak, for a few minutes, the flare nearly outshines the star's photosphere. A detailed analysis of the flare's decay, however, shows that this is an interesting event also on other accounts. Typical loop lengths derived for strong flares on active stars, mostly using the quasi-static cooling mechanism, are large, comparable or often greater than the stellar radius. The picture which has emerged from most of the literature is thus one of long, tenuous plasma structures, with the attendant challenges of sufficiently strong magnetic fields far away from the stellar surface. In the present case, instead, the loop semi-length derived from the analysis of the flare decay using the method of Reale et al. (1997) is relatively compact, at about 0.5 stellar radii (implying a maximum height above the stellar surface of $\simeq 0.3$ stellar radii). The length derived using the quasi-static formalism is about 4 times larger, and would thus again lead to the "classic" picture of long, tenuous loops.

Although certainly not small, flaring loops of $L \simeq 0.5\ R_*$ are by no means exceptional, even by the relatively modest solar standards. The analysis of the large flare on Algol seen by the SAX observatory (Schmitt & Favata 1999; Favata & Schmitt 1999) shows that the picture of large tenuous loops implied by the results of the quasi-static analysis can be quite misleading, and that, at least in that case, the geometrical size of the flaring plasma constrained by the light-curve eclipse is significantly smaller than the loop heights derived with the quasi-static method. An analysis based on the method of Reale et al. (1997) yields, also in that case, loop dimensions which are significantly smaller than the ones implied by the quasi-static analysis. The much more compact loop size derived through the Reale et al. (1997) method is linked with the presence of significant plasma heating during the flare decay, as the implied small, dense loop has a very short thermodynamic decay time ($\tau_{\rm th} \simeq 400$ s). No large diffuse plasma structures at several stellar radii from the surface are needed to model the flaring region, and a more appropriate picture appears to be one of a rather compact, high-pressure plasma structure, whose decay is completely dominated by the time-evolution of the heating mechanism.

The present large EV Lac flare shows several characteristics in common with other large, well observed stellar flares discussed in the literature. The light curve has a "double exponential" decay, with the initial time scale being more rapid, and a slower decay setting in afterwards. A very similar decay pattern is observed in the large Algol flare seen by SAX as well as on many large solar flares (see Feldman et al. 1995 for an example). The best-fit metal abundance for the flaring plasma also shows what by now appears to be a characteristic behavior, i.e. it increases in the early phases of the flare, peaking more or less with the peak of the light-curve, and then it decreases again to the pre-flare levels. In the case of the SAX Algol flare the long duration of the event and the high intensity of the flare make it possible to show that the metallicity decays to its pre-flare value on faster time scales than either the plasma temperature or the emission measure. The coarser time coverage of the present flare and the shorter duration of the event do not allow such detailed assessment.

The heating mechanism of the solar (and stellar) corona remains in many respects an unsolved puzzle, and even more the mechanism responsible for large flares. However, it is by now rather clear that most sizable flares cannot be explained with a simple picture of a (mostly) impulsive heating event followed by decay dominated by the free thermodynamic cooling of the plasma structure. On the contrary, the evidence from the recent flow of well studied flare data (including the one in the present paper) is that the decay of large flares is dominated by the time evolution of the heating mechanism. Thus, the double exponential decay observed here as well as in other large solar and stellar flare is likely to be a characteristic of the heating mechanism rather than one of the flare decay.

The interpretation of the increase in best-fit plasma metallicity during the flare's peak is still unclear. If the presence of a fractionation mechanism is accepted, which causes differences in the metal abundances in the photosphere and in the corona, the abundance increase during the flare can plausibly be explained as due to the evaporation of photospheric plasma during the early phases of the flare, on time scales faster than the ones on which the fractionation mechanism operates. Since the coronal plasma shortly after the impulsive heating is almost entirely made of material evaporated from the chromosphere, if this scenario were correct the observations presented here would imply that the chromospheric metallicity should be about three times the coronal one in quiescent conditions.

Recent calculations (G. Peres, private communication) show that the plasma in a flaring loop such as the one responsible for the EV Lac flare discussed here is not optically thin for the strongest lines. This is in particular true for the Fe XXV complex at $\simeq 6.7$ keV, which drives the determination of the metallicity of the flaring plasma. However, optical thickness effects would in general depress the strong line, leading to a lower metallicity estimate, and cannot therefore explain the metallicity increase observed during the flare. Another possible bias to the best-fit metallicity can derive from the thermal structure of the flaring plasma, which is not isothermal, even if it's being fit with an isothermal model. To assess the magnitude of this effect we analyzed the synthetic spectra produced with an ad hoc hydrodynamic simulation of a flaring loop, showing that the effect is small ($\leq 30\%$) in comparison with the observed magnitude of the change (a factor of $\simeq 3$).

If the heating mechanism responsible for the present flare is essentially due to some form of dissipation of magnetic energy, an obvious question to ask is what field strength would be required to accumulate the emitted energy, and to keep the plasma confined in a *stable* magnetic loop configuration. A related question is whether the present flare could be interpreted with a reasonable scaling of the conditions usually observed in the solar corona, or whether a different configuration and/or mechanism for energy release need to be invoked. Our flare analysis allows to make some relevant estimates, under the assumptions that the energy release is indeed of magnetic origin and it occurs entirely within a single coronal loop structure, with the characteristics inferred from the analysis of the flare decay. An estimate of the minimum magnetic field $B$ necessary to produce the event can then be obtained from the relation:

$$E_{\rm tot} = \frac{(B^2 - B_0^2) \times V_{\rm loop}}{8\pi} \qquad (11)$$

where $E_{\rm tot} \simeq 7 \times 10^{34}$ erg is the total energy released (Sect. 3.3), $B_0$ is the magnetic field surviving the flare and $V_{\rm loop}$ is the total volume of the flaring plasma. As an estimate of $B_0$ we take the magnetic field necessary to maintain the plasma confined in a rigid loop structure along the whole flare, thus implicitly assuming that the loop geometry does not change during the flare. From a plasma density $n \simeq 2 \times 10^{12}$ cm$^{-3}$, and a temperature $T \simeq 100$ MK the estimated maximum plasma pressure is $6 \times 10^4$ dyn cm$^2$; in order to support such a pressure, a field of $\simeq 1.2$ kG is required. Hence, the total minimum magnetic field required to explain the flare is, from Eq. 11, $B \simeq 3.7$ kG, a value compatible with the average magnetic field of 3.8 kG, with a surface filling factor of about 60% (and evidence for field components of up to $\simeq 9$ kG), measured on EV Lac by Johns-Krull & Valenti (1996) at photospheric level.

Although we have used the loop volume in the derivation of $B$, this is not to say that the field fills up the whole volume. Rather, our estimates can be interpreted in the framework of the flare energy stored in a magnetic field configuration (e.g. a large group of spots) with a field strength of several kG, covering a volume comparable to the one of the flaring loop. What rests as a matter of speculation is how often such a large energy release may occur, or in other words, what are the conditions required to accumulate such large amounts of magnetic energy, especially when the photosphere is so permeated of magnetic fields as shown by Johns-Krull & Valenti (1996).

In any case, the above scenario suggests the presence of large-scale, organized magnetic fields. This is somewhat in contrast with the hypothesis that EV Lac is a fully convective star, whose activity is powered by a turbulent dynamo, which would be expected to produce small-scale magnetic fields. Most dynamo theories suggest (Durney et al. 1993) that less magnetic flux should be generated by a turbulent dynamo (as compared to the case of the solar-type "shell" dynamo) because there is no stable overshoot layer where the fields can be stored and amplified, and only small-scale magnetic regions should emerge uniformly to the surface, because the crucial ingredient is small-scale turbulent flow field, rather than large-scale rotational shear.

On the other hand the presence of a magnetic field may substantially modify the stellar interior structure. Magnetic fields – even smaller than dictated by equipartition arguments – alter the convective instability conditions (Ventura et al. 1998), and thus likely modify the structure of the convective envelope. At the same time convection has the tendency to pump magnetic fields downward ("turbulent pumping"; Brandenburg et al. 1992; Tobias et al. 1998), so that – in a fully-convective star – fields may accumulate near the center. Hence, magnetic fields are likely to be an important (and thus far essentially unaccounted) term in determining the actual stellar structure, and any realistic calculation at the low-mass end should consider the dynamo-generated magnetic fields as an essential part. Indeed, the possibility that a strong magnetic field can lead to the formation of a radiative core has been discussed by Cox et al. (1981), and this may be the seed for a resurrection of a "shell" dynamo mechanism.

*Acknowledgements.* We would like to thank J. Schmitt for the helpful discussion relative to the choice of the best target for this observing program, and G. Peres and S. Orlando for the illuminating discussions on many details of flare evolution. FR, GM, SS and AM acknowledge the partial support of ASI and MURST.

## References

Ambruster C., Snyder W. A., Wood K. S. 1984, ApJ 284, 270
Ambruster C. W., Sciortino S., Golub L. 1987, ApJS 65, 273
ASCA ABC Guide 1997, The ASCA Data Reduction Guide, ASCA Guest Observer Facility, Laboratory for High Energy Astrophysics, NASA/Goddard Space Flight Center, 2.0 edition
Baraffe I., Chabrier G., Allard F., Hauschildt P. H. 1998, A&A 337, 403
Barbera M., Micela S., Sciortino S., Harnden, F.R. J., Rosner R. 1993, ApJ 414, 846
Brandenburg A., Moss D., Tuominen I. 1992, in The Solar Cycle, Vol. 27 of ASP Conference Series, 536
Brickhouse N. S. 1998, in R. Donahue, J. Bookbinder (eds.), 10th Cambridge Workshop on Cool Stars, Stellar Systems and the Sun, Vol. 154 of ASP Conf. Series, ASP, San Francisco, p. 487
Chabrier G., Baraffe I. 1997, A&A 327, 1039
Cox A. N., Shaviv G., Hodson S. W. 1981, ApJ 245, L37
Delfosse X., Forveille T., Perrier C., Mayor M. 1998, A&A 331, 581
Durney B. R., de Young D. S., Roxburgh I. W. 1993, Solar Phys. 145, 207
Favata F., Schmitt J. H. M. M. 1999, A&A in press
Feldman U., Seely J. F., Dosheck G. A. et al. 1995, ApJ 446, 860
Fleming T. A., Schmitt J. H. M. M., Giampapa M. S. 1995, ApJ 450, 401
Haisch B. M. 1983, in P. B. Byrne, M. Rodonò (eds.), Activity in red dwarf stars, Vol. 102 of Astrophysics and Space Science Library, 255
Houdebine E. R., Foing B. H., Doyle J. G., Rodonò M. 1993, A&A 278, 109
Johns-Krull C. M., Valenti J. A. 1996, ApJ 459, L95
Kopp R. A., Poletto G. 1984, Sol. Phys. 93, 351
Maggio A., Peres G. 1997, A&A 325, 237
Mewe R., Kaastra J. S., Liedahl D. A. 1995, Legacy 6, 16
Pallavicini R., Tagliaferri G., Stella L. 1990, A&A 228, 403
Pettersen B. R., Olah K., Sandmann W. H. 1992, A&AS 96, 497
Poletto G., Pallavicini R., Kopp R. A. 1988, A&A 201, 93

Reale F., Betta R., Peres G., Serio S., McTiernan J. 1997, A&A 325, 782
Reale F., Micela G. 1998, A&A 334, 1028
Reale F., Peres G., Serio S., Rosner R., Schmitt J. H. M. M. 1988, ApJ 328, 256
Reale F., Serio S., Peres G. 1993, A&A 272, 486
Reid I. N., Hawley S. L., E. G. J. 1995, AJ 110, 1838
Roizman G. S., Shevchenko V. S. 1982, Sov. Astr. Letters 8, 85
Rosner R., Tucker W. H., Vaiana G. S. 1978, ApJ 220, 643
Schmitt J. H. M. M. 1994, ApJS 90, 735
Schmitt J. H. M. M. 1998, in R. A. Donahue, J. A. Bookbinder (eds.), Cool Stars, Stellar Systems and the Sun, Vol. 154 of ASP Conference Series, ASP, San Francisco, 463
Schmitt J. H. M. M., Favata F. 1999, Nat 401, 44
Schmitt J. H. M. M., Fleming T. A., Giampapa M. S. 1995, ApJ 450, 392
Schmitt J. H. M. M., Kurster M. 1993, Science 262, 215
Schmitt J. H. M. M., Rosso C. 1985, A&A 191, 99
Sciortino S., Maggio A., Favata F., Orlando S. 1999, A&A 342, 502
Serio S., Reale F., Jakimiec J., Sylwester B., Sylwester J. 1991, A&A 241, 197
Stern R. A., Uchida Y., Tsuneta S., Nagase F. 1992, ApJ 400, 321
Sylwester B., Sylwester J., Serio S. et al. 1993, A&A 267, 586
Tobias S. M., Brummell N. H., Clune T. L., Toomre J. 1998, ApJ 502, L177
van den Oord G. H. J., Mewe R. 1989, A&A 213, 245
Ventura P., Zeppieri A., Mazzitelli I., D'Antona F. 1998, A&A 331, 1011
Wu S. T., de Jager C., Dennis B. R. et al. 1986, in M. Kundu, B. Woodgate (eds.), Energetic phenomena on the Sun, No. 2439 in NASA Conference Publication, NASA, p. 5

## Appendix A: Physical characteristics of EV Lac

EV Lac (Gl 873) is a dMe dwarf, classified as M3.5 (Reid et al. 1995), at a distance (from the Hipparcos-measured parallax) $d = 5.05$ pc. It is considered a single star, with no evidence of companions, and is a slow rotator, with a photometrically determined rotation period of 4.378 d (Pettersen et al. 1992). The projected equatorial velocity has been determined from Doppler broadening of the spectral lines at $v \sin i = 4.5 \pm 0.5$ km s$^{-1}$ (Johns-Krull & Valenti 1996) and $v \sin i = 6.9 \pm 0.8$ km s$^{-1}$ (Delfosse et al. 1998); this rotation velocity can be reconciled with the observed starspot modulation period only if the inclination is high ($\geq 60$ deg). The rotational velocity of M dwarfs (Delfosse et al. 1998) is characterized by the bulk of them having a narrow distribution with $v \sin i \leq 5$ km s$^{-1}$, and a tail of rare fast rotators with velocities of up to $\simeq 50$ km s$^{-1}$. EV Lac lies at the upper end of the slow-rotator distribution.

The absolute magnitude is $M_V = 11.73$, which, given a color index $(R - I)_{\rm C} = 1.52$ translates in $M_{\rm bol} = 9.40$ (Delfosse et al. 1998), corresponding to $L_{\rm bol} = 5.25 \times 10^{31}$ erg s$^{-1}$. Using the mass-luminosity relationship of Baraffe et al. (1998) and the $K$-band luminosity (to be preferred given the independence of the relationship between mass and $K$-band luminosity from metallicity) $M_K = 6.78$ (Delfosse et al. 1998) we derive a mass of $\simeq 0.35 M_\odot$. No photospheric abundance analyses of EV Lac are known to us, although Fleming et al. (1995) report a near-solar metallicity based on broad-band photometry. The radius for a solar-metallicity $0.35 M_\odot$ dwarf is, from the models of Chabrier & Baraffe (1997), $R \simeq 2.5 \times 10^{10}$ cm, or $R \simeq 0.36 R_\odot$, (assuming the star is old enough, given that such a low-mass star will contract gravitationally until it's $\simeq 300$ Myr old).

Stellar structure models show that the radiative core of low-mass stars shrinks with decreasing mass, disappearing completely in mid-M dwarfs, so that late-M dwarfs are expected to be completely convective. Solar-type dynamos are thought to require an interface between the convective envelope and the radiative core (the $\alpha$–$\Omega$ shell dynamo model) and are thus not expected to be present in the cooler M dwarfs. Given that however X-ray activity is present and common even in purportedly fully convective late M dwarfs (Barbera et al. 1993; Schmitt et al. 1995) a different type of dynamo mechanism must be operating in them; it has recently been suggested that small-scale magnetic fields can be generated in convection zones by a turbulently driven dynamo (Durney et al. 1993). This – which could be also at work in higher mass stars with varying degrees of efficiency, depending on the rotation rate – would therefore provide the only magnetic field generation mechanism in fully convective low-mass dwarfs.

The predicted mass at which stars become fully convective depends on the details of the physics adopted in the stellar models. Chabrier & Baraffe (1997) use non-grey atmospheres to put the fully convective limit at $0.35 M_\odot$ (i.e. just at the estimated mass of EV Lac), independent of metallicity in the range $0.01 Z_\odot < Z < Z_\odot$. Different calibrations for the mass-luminosity relationships (see discussion in Delfosse et al. 1998) push the fully-convective limit toward somewhat higher masses, so that EV Lac is most likely fully convective, and thus its activity is likely to be driven purely by a turbulent dynamo, which is not, among other things, expected to have a solar-like cyclic behavior, and which is expected to generate magnetic fields on a smaller spatial scale (related to the scale of the turbulent flow fields) than an $\alpha$–$\Omega$ dynamo. The picture is complicated by the fact that strong magnetic fields may influence the stellar interior structure maintaining a radiative core at masses lower than the theoretical limits for spherically symmetric, non-magnetic stars (Cox et al. 1981), and thus the magnetic fields of very active, low-mass stars could still be (partially) powered by an $\alpha$–$\Omega$ shell dynamo.

### *A.1. Previous X-ray observations*

The high activity of EV Lac had been noted well before the advent of high-energy observations from its large optical and UV flaring rate, with some truly exceptional optical flares observed: Roizman & Shevchenko (1982) report the occurrence of a 6.4 mag $U$-band flare, lasting 6.4 hr, with a peak luminosity of $\simeq 10^{32}$ erg s$^{-1}$ and a total energy output of $\geq 10^{35}$ erg.

EV Lac was first observed as a quiescent soft X-ray source by EXOSAT (Schmitt & Rosso 1985) – although it had been detected earlier by HEAO-1 during a strong flare with $\log L_{\rm X} = 28.7$ erg s$^{-1}$. It was not observed by the *Einstein* observatory, while it was observed by ROSAT both in the All Sky Survey (in which a major flare was also detected) and in pointed mode. The RASS quiescent X-ray luminosity was $\log L_{\rm X} = 29.08$ erg s$^{-1}$ (Schmitt et al. 1995), corresponding to $\log L_{\rm X}/L_{\rm bol} = -2.6$. It was also the subject of one SAX and several PSPC pointings, analyzed in Sciortino et al. (1999), during which its coronal emission shows both a continuous variability of about a factor 2–3 and the occurrence of an intense flare, with an increase of the emission in the PSPC of about 10-fold.

The HEAO A-1 Sky Survey experiment (Ambruster et al. 1984) detected two flares from EV Lac, with peak X-ray luminosities (in the 0.5–20 keV band) of $\log L_{\rm X} = 29.5$ erg s$^{-1}$ and $\log L_{\rm X} = 30.3$ erg s$^{-1}$. The most energetic of the two flares represented a peak enhancement of $\simeq 50$ over the quiescent X-ray luminosity ($L_{\rm X} \simeq 10^{28.5}$ erg s$^{-1}$), and its decay $e$-folding time was roughly estimated to be of the order of $\leq 5$ ks (although the very sparse temporal coverage prevents an accurate determination of the flare's decay). Ambruster et al. (1984) have also estimated the physical parameters of the two flares (*assuming* a peak temperature of $\simeq 2 \times 10^7$ K), resulting, for the smaller of the two flares, in a peak emission measure $EM \simeq 2 \times 10^{53}$ cm$^{-3}$, a density $n \simeq 5 \times 10^{11}$ cm$^{-3}$ and a loop length $L \simeq 5 \times 10^9$ cm. The magnetic field strength necessary to confine the plasma was estimated at $200\ G$. Only the peak emission measure is reported for the second flare ($EM \simeq 2 \times 10^{53}$ cm$^{-3}$). A small flare was seen in one of the EXOSAT observations, in the LE detector, as discussed in detail by Pallavicini et al. (1990). Its rise time ($1/e$ time) was $\simeq 600$ s, and its decay time was $\simeq 4.5$ ks. At peak the flare represented an enhancement of only $\simeq 3$ times over the quiescent X-ray flux, with a peak X-ray luminosity $L_{\rm X} \simeq 10^{29}$ erg s$^{-1}$ and a total energy released in the X-rays $E \simeq 10^{32}$ erg. The lack of energy resolution of the EXOSAT LE detector made it impossible to perform an analysis of the flare's decay.

Schmitt (1994) derived loop parameters for the long RASS flare by fitting the flare decay parameters within the framework of the quasi-static formalism of van den Oord & Mewe (1989). The maximum observed temperature is $T \simeq 30$ MK, the decay timescale is $\tau \simeq 38$ ks, and the peak emission measure is $EM \simeq 1.5 \times 10^{52}$ cm$^{-3}$. The loop length derived through a quasi-static analysis is large, at $L \simeq 6 \times 10^{11}$ cm $\simeq 10\ R_*$ (with an inferred flaring volume $V \simeq 3 \times 10^{31}$ cm$^3$) and the plasma density is correspondingly low, at $n \simeq 3 \times 10^{10}$ cm$^{-3}$. The total thermal energy was estimated at $E \simeq 9 \times 10^{34}$ erg. Schmitt (1994) also analyzed the EV Lac PSPC flare decay using the two-ribbon model of Kopp & Poletto (1984) finding that (as originally discussed by Poletto et al. 1988) while this framework can in principle yield a reasonable fit to the observed light curve, it does not allow to distinguish between a low-density plasma organized on large spatial scales from a compact high-density plasma, thus yielding little physical insight in the structure of the flaring region.